Spectroscopy and thermodynamics of ArHCl

Lawrence S. Bernstein and Joda Wormhoudt

Citation: The Journal of Chemical Physics **80**, 4630 (1984); doi: 10.1063/1.446548
View online: http://dx.doi.org/10.1063/1.446548
View Table of Contents: http://scitation.aip.org/content/aip/journal/jcp/80/10?ver=pdfcov
Published by the AIP Publishing

Spectroscopy and thermodynamics of ArHCl

Lawrence S. Bernstein
Spectral Sciences, Inc., Burlington, Massachusetts 01803

Joda Wormhoudt
Aerodyne Research, Inc. Billerica, Massachusetts 01821

(Received 21 October 1983; accepted 6 February 1984)

A general model for analysis of the infrared spectrum of atom–diatom van der Waals molecules is developed. Using energy levels and spectroscopic parameters based on the Hutson and Howard M5 potential, this model quantitatively reproduces the previously observed ArHCl spectrum in the null gap of the monomer HCl spectrum. The thermodynamics of atom–atom and atom–diatomic systems is discussed. An approximate quantum mechanical method of evaluating bound and metastable partition functions is derived. Simple expressions for the partition functions are given which are shown to accurately reproduce the well established results for atom–atom complexes. The generalization of the approach to atom–diatomics is discussed. These partition functions are used to calculate thermodynamic properties such as heat capacities and equilibrium constants.

I. INTRODUCTION

Much can be learned about the intermolecular potential energy surfaces of van der Waals molecules from analysis of their infrared spectra.[1–15] Resolved line spectra have been observed for complexes composed of light monomers such as ArH_2. LeRoy and co-workers[1,2] have shown that the entire anisotropic potential surface can be determined from analysis of such spectra. When the complex is composed of heavier monomers, such as in ArO_2, the lines cannot be resolved and smooth band contours are observed. Ewing and coworkers [4,6,14,15] have devised a band contour synthesis approach which has proved useful in revealing major features of the potential surfaces for heavier complexes.

In this paper, a general band contour model is developed for atom–diatomic complexes. This model is used to analyze the previously observed ArHCl absorption spectrum in the null gap of the monomer HCl spectrum.[16–19] In previous applications of band contour modeling the parameters of the potential were varied to yield a best fit to the observed spectrum. ArHCl is of particular interest because its full anisotropic potential surface is well determined. Thus, analysis of the ArHCl spectrum provides a unique opportunity to refine the band contour modeling approach.

The ArHCl potential surface used in this study is the Hutson and Howard M5 potential.[20,21] Their surface was constrained to reproduce a wide variety of experimental data which were sensitive to different aspects of the potential. The ArHCl dissociation energy was determined to be 181 cm^{-1}. This value is much lower than previous estimates of the dissociation energy based on analysis of infrared spectra.

Miziolek and Pimentel[18] analyzed the temperature dependence of the peak absorption features in their ArHCl infrared spectra and estimated a dissociation energy of 420 cm^{-1}. Their analysis was based on the assumption that the peak spectral absorption coefficients were temperature independent. Boom and van der Elsken [22–24] reanalyzed these data incorporating a temperature dependence based on a single absorbing transition and lowered the estimated dissociation energy to 233 cm^{-1}. In the present study, the ArHCl spectrum is shown to be composed of many overlapping transitions. When the positions and intensities of these transitions are based on the M5 potential, the synthetic spectra quantitatively reproduce the entire experimentally observed spectrum and its temperature dependence.

Classical and quantum mechanical methods for calculating thermodynamic properties of atom–atom systems are well established.[25–27] This is not the case for atom–diatomic complexes.[28] The additional degree of freedom due to the librational motion of the diatomic makes these calculations significantly more complicated. Although accurate methods[1–3,21,22,27–33] have been developed to calculate eigenvalues for atom–diatomic potentials, they have not been adapted for routine use in determining the full manifold of eigenvalues needed for the partition function. This is not a serious limitation because thermodynamic properties involve averages over many levels and great accuracy is not required for each level. Accurate partition functions can be determined using approximate energy level distributions that preserve the correct total number of bound states supported by the potential. This is demonstrated here using an approximate quantum mechanical method which is applied to both atom–atom and atom–diatomic systems.

II. ENERGY LEVELS AND SPECTROSCOPIC PARAMETERS

Hutson and Howard[20] have shown that the ArHCl potential has two minima corresponding to linear structures. These structures are separated by a 76 cm^{-1} barrier, and the ArHCl configuration is 35 cm^{-1} more stable than the ArClH configuration. One expects the infrared spectrum of the lowest energy state for each minimum to resemble a parallel band for a linear triatomic molecule. Since the ArHCl spectra were taken at temperatures comparable to the ArHCl bond energy they are composed of overlapping band contours from many excited vibration-libration states.

 0021-9606/84/104630-10$02.10

Only ArHCl parallel band transitions will occur with significant intensity in the null gap region of the monomer HCl spectrum. These transitions fall within the null gap because their spectral location is determined by the sum of the HCl fundamental frequency plus (and minus) a small rotational contribution from the overall complex. The rotational contribution is small because the ArHCl rotational constant is small, $B_0 = 0.056\ \mathrm{cm}^{-1}$. Bratoz and Martin[34] have shown that as the librational motion of the HCl approaches that of a free rotor the parallel band transitions become forbidden. One also expects dimer transitions which include a change in the librational state to be quite strong, since in the free rotor limit they correspond to the monomer HCl transitions. However, based on the predicted large energy differences between the librational levels[20] these transitions are not expected to fall within the null gap region.

The above considerations motivated a simplified spectral model whose major assumptions are:

(1) The selection rules, line positions, and strengths are those for a parallel band of a linear molecule with the spectroscopic constants and intensity factors appropriately averaged over the large amplitude bending and stretching motions.
(2) The stretching energy levels and rotational constants of the complex are estimated from a Lennard-Jones potential.
(3) The librational motion below the barrier to free rotation is approximated as an isotropic two-dimensional harmonic oscillator.
(4) Only librational states below the free rotation barrier contribute to the null gap spectrum.
(5) The ArHCl integrated band strength is determined by the unperturbed monomer HCl integrated band strength.

These approximations are used to determine the energy levels and spectroscopic constants for each of the linear configurations.

A. Line positions and strengths

For ArHCl transitions where one quantum of vibrational energy is absorbed by the HCl, the line locations are modeled by

$$\omega = \omega_\eta + 2B_\eta m - \alpha_\eta m^2 - 4D_\eta m^3 + 6H_\eta m^5, \qquad (1)$$

where ω_η is the band center for the η stretching vibrational state, and the rotational constants $B_\eta, \alpha_\eta, D_\eta, H_\eta$ have the standard definitions.[35] The quantity m is defined in terms of the total angular momentum quantum label l by $m = -l$ and $l+1$ in the P and R branches, respectively. Because of the large amplitude stretching motion, the coefficients in Eq. (1) depend strongly on the η quantum state. The variation of these coefficients due to the large amplitude bending motion is much smaller and is not included in the present model. This is because the equilibrium bond length varies slowly with the bending angle in the region about each linear configuration.

The line strength for a parallel band transition[35] is approximated by

$$S = S_0 \langle \cos\theta \rangle^2_{\eta j} |m| \exp(-G_{\eta j l}/kT)/Q, \qquad (2)$$

where S_0 is the integrated band strength of monomer HCl, j is the librational quantum number, $\langle \cos\theta \rangle$ is the average of $\cos\theta$, θ is the angle between the HCl and the line joining the Ar to the HCl center-of-mass, G is the lower state energy, and Q is the dimer partition function.

While some change in the monomer HCl band strength, or equivalently its dipole moment derivative, will occur due to formation of the ArHCl complex, this change is expected to be small. Because of the large amplitude bending the projection of the HCl dipole moment derivative along the bond axis is considerably smaller than unity (this projection determines the total strength of the parallel band). This effect is modeled by the $\langle \cos\theta \rangle^2$ factor.

Accuracy requirements for the spectral parameters in Eqs. (1) and (2) can be established from consideration of the low spectral resolution and uncertainties in the absolute values of the measured ArHCl absorption coefficients. The uncertainties in the absolute values arise from uncertainties in the instrument baseline and subtraction of the underlying continuum due to the wings of distant monomer HCl lines. Since line structure was not observed, a sensible accuracy requirement is that the location of key spectral features, such as the P and R branch peaks, are accurate to within a few line spacings. For ArHCl this is approximately a $0.2\ \mathrm{cm}^{-1}$ uncertainty and corresponds to an uncertainty in the rotational constant B_η of 10%. The absorption coefficient is proportional to the line strength and from Eq. (2) an uncertainty in the lower state energy of ΔG produces an uncertainty in the line strength of $\Delta G/kT$. Because the measurement temperature regime was relatively high ($200 < T < 300\ K$) a large uncertainty in the lower state energy, $\Delta G = 10\ \mathrm{cm}^{-1}$, results in about 5% uncertainty in the absorption coefficient. The expressions for the spectral parameters which are presented below are believed to be consistent within the accuracy limits just discussed. Conclusive justification of this assertion requires accurate computations of energy levels and wave functions, which is far beyond the scope of the present effort.

B. Energy levels and spectroscopic parameters

The energy levels are represented by

$$G_{\eta j l} = G_\eta + B_\eta l(l+1) - D_\eta l^2(l+1)^2 + H_\eta l^3(l+1)^3 + f_\eta \omega_b (j+1), \qquad (3)$$

where G_η is the stretching vibrational energy, ω_b is the bending energy for the ground stretching state, and f_η accounts for the coupling of the bending and stretching motions ($0 \leqslant f_\eta \leqslant 1$). For a Lennard-Jones (12-6) potential Cashion[27] has determined simple and accurate formulas for the vibrational energy levels and the rotational coefficients. Cashion's formulas are summarized in Table I in nondimensionalized form, making use of the reduced quantum number

$$\xi = (\eta_D - \eta)/(\eta_D + 1/2), \qquad (4)$$

where η_D is the quantum number at the dissociations limit. Although Cashion's formulas are specific to the LJ (12-6) potential they can be approximately scaled for a general LJ (n-6) potential simply by using the value of η_D appropriate for the value of the repulsive wall exponent n. Mahan[26] has

TABLE I. Energy level expansion coefficients for a Lennard-Jones (12-6) potential.[a]

X	$= 1 - \xi$
G_η	$= (2.8620\times10^{-3})\epsilon X(1000.0 - 904.31X + 212.68X^2 + 32.919X^3 + 7.5491X^4 + 1.4190X^5 + 0.15409X^6 - 1.0012X^7)$
B_η	$= (1\times10^{-3})B_e(1000.0 - 715.50X - 203.83X^2 - 72.268X^3 - 20.605X^4 - 8.0012X^5 + 24.65X^6)$
D_η	$= (1\times10^{-3})D_e(1000.0 + 2583.8X + 3835.3X^2)$[b]
H_η	$= (1\times10^{-3})H_e(1000.0 + 5946.0X)$[c]

[a] Only the leading term for each order is shown. This leads to an error of order $100\,(B_e/\omega_e)^2$ which is typically around 10^{-4} (Ref. 27).
[b] D_e can be estimated from $D_e = 0.0278\,(B_e^2/\epsilon)\,(\mathrm{cm}^{-1})$ (Ref. 27).
[c] H_e can be estimated from $H_e = 0.003\,09\,(B_e^3/\epsilon^2)\,(\mathrm{cm}^{-1})$ (Ref. 27).

derived a general relationship between η_D and n which is well approximated by

$$\eta_D + 1/2 = 0.2385\sqrt{(\epsilon/B_e)(12/n)}, \tag{5}$$

where ϵ is the equilibrium dissociation energy and B_e is the equilibrium rotational constant for the complex.

There is a simple and accurate approximation to the expansion for G in Table I that is useful for scaling quantities which can be expressed in terms of the potential energy function. It is given by

$$G_\eta = \epsilon(1 - \xi^3). \tag{6}$$

This approximation originates from the work of LeRoy and Bernstein[36] on the spacing of levels near dissociation. While this approximation is very accurate for higher lying levels it is still reasonably accurate even for the lowest lying levels. For ArHCl, the ground state energy as determined by this approximation differs by about 1 cm^{-1} from that calculated with the expansion formula.

The M5 potential is approximated as the product of an angular function and an LJ (n-6) potential. This means that an effective bending force constant can be defined for each stretching state and that it is proportional to $\epsilon - G_\eta$ and therefore ξ^3. Since the bending energy scales with the square root of the force constant the expression for the coupling constant in Eq. (3) is given by

$$f_\eta = \xi^{3/2}. \tag{7}$$

For a harmonic oscillator the average of the square of the vibrational amplitude is inversely proportional to the square root of the force constant. This enables the quantity $\langle\cos\theta\rangle^2$ to be scaled from its ground state value through

$$\langle\theta^2\rangle_{\eta j} = \langle\theta^2\rangle_{00}\xi^{-3/2}(j+1), \tag{8}$$

where $\langle\theta^2\rangle_{00}$ is defined by the value of θ consistent with the measured quantity $\langle P_1(\cos\theta)\rangle$.[21]

The vibration-rotation constant α_η in Eq. (1) accounts for the small change in the effective Ar to HCl center of mass distance due to the increase in the effective HCl bond length with vibrational excitation of the HCl. Although α_η is small, it can have a significant affect on the location of high "m" lines because of the m^2 weighting in Eq. (1). This quantity is not known for ArHCl, but an upper limit can be established by assuming the change in the ArHCl center of mass distance is equal to the change in the HCl bond length. This results in

$$\alpha_\eta = \alpha_d(r_e/R_e)(B_0/B_d)\xi^{3/2}, \tag{9}$$

where α_d is the vibration-rotation constant for HCl, r_e is the HCl equilibrium bond length, R_e is the Ar–HCl equilibrium center of mass distance, and B_d is the HCl rotational constant. This approximation yields values for the rare gas–H2/D2 complexes which are in reasonable agreement with the detailed theoretical results of Leroy and van Kranendonk.[1]

Usually there is a small shift to lower wave number of the vibrational frequency of a diatomic molecule complexed to a rare gas atom. Previous work on matrix induced shifts model the shift as roughly proportional to the potential.[37] Again, making use of Eq. (6), the dependence of the shift on the stretching state is given by

$$\omega_\eta = \omega_e + \Delta\omega_0\xi^3, \tag{10}$$

where ω_e is the unperturbed HCl vibrational frequency and $\Delta\omega_0$ is the shift for the $\eta = 0$ stretching state.

There are a finite number of dimer rotational states which can contribute to the spectrum. Two distinct upper limits must be considered, given by the numbers of bound and metastable rotational levels. Mahan[26] has shown that these limits are given by

$$l_\eta^b = \xi\sqrt{\epsilon/B_e} \tag{11}$$

and

$$l_\eta^m = l_\eta^b\sqrt{1+\delta}, \tag{12}$$

where l_η^b and l_η^m correspond to the bound and metastable upper limits. The quantity δ is a constant which depends only on the repulsive wall exponent for an LJ (n-6) potential. By parameterizing Mahan's calculations δ is given by

$$\delta = 1.37 - 8.45/n. \tag{13}$$

This predicts a value of $\delta = 0.667$ for $n = 12$ which is significantly different from the value of $\delta = 0.357$ used by Stogryn and Hirschfelder.[25] We are not aware of the source of this discrepancy.

Mahan's results apply to an atom–atom potential, and require modification for an atom–diatom potential. This is because the dissociation energy depends on the orientation of the diatomic. Within the harmonic oscillator approximation to the bending motion, the reduction in the dissociation energy is equal to the average of the bending potential. Then an effective dissociation energy can be used in Eq. (11) and Eq. (12) which is given by

$$\epsilon' = \epsilon - f_\eta(\omega_b/2)(j+1), \tag{14}$$

where, as before, ϵ is the equilibrium dissociation energy for each linear configuration.

The metastable rotational states have finite lifetimes[25] which can lead to appreciable broadening of the transitions. While this effect can significantly alter the appearance of a highly spectrally resolved spectrum, it is of secondary importance when the spectral resolution or other line broadening effects are large compared to lifetime broadening. This is the case for the ArHCl spectra analyzed here, and the full line strength for each metastable transition will contribute to the observed spectral contour.

III. CALCULATION OF DIMER SPECTRA

A. General considerations

The observed dimer absorption spectra can be expressed as the sum of three terms,

$$-\ln(I/I_0) = \rho_{AB}\sigma_{AB}l + \rho_A\rho_B\sigma_c l + \tau, \quad (15)$$

where I_0 is the incident light, I is the transmitted light, ρ_{AB} is the dimer density, σ_{AB} is the dimer absorption cross section, l is pathlength, ρ_A and ρ_B are monomer densities, σ_c is the absorption cross section due to collision broadening of monomer lines, and τ is the total absorption loss due to instrument optical components.

The dimer density is related to the dimer equilibrium constant K_{eq} by

$$\rho_{AB} = \rho_A\rho_B K_{eq}. \quad (16)$$

For the general case where A is an atom and B is a diatomic molecule, the equilibrium constant is given by

$$K_{eq} = \exp(\epsilon/\kappa T)\,(h^2/2\pi\mu kT)^{3/2} Q_{AB}(hcB_d/kT), \quad (17)$$

where μ is the reduced mass and Q_{AB} is the dimer partition function.

Calculation of the absorption cross section at each spectral location involves summing over all transitions. The contribution of each transition is proportional to the product of its line strength with an appropriate line shape function. When the spacing between lines is less than the effective linewidth it is not necessary to calculate the spectrum on a line-by-line basis. (The effective linewidth is the convolution of the instrument resolution with the pressure and lifetime broadened linewidths.) In this limit a simpler and nearly as accurate an approach is to determine a local average cross section through

$$\sigma_{AB} = \sum_i S_i/\Delta\omega, \quad (18)$$

where the line strength summation is over all lines in the interval from ω to $\omega + \Delta\omega$. The line strength varies relatively slowly with wave number and the average absorption coefficient is insensitive to the exact value of $\Delta\omega$. It is useful to keep $\Delta\omega$ small compared to the effective instrument resolution so that further averaging over an instrument spectral response function can be performed.

We note that it is not necessary to evaluate the dimer partition function in order to calculate dimer spectra. This is because the dimer absorption is proportional to the product of line strength [Eq. (2)] and equilibrium constant [Eq.(17)] in which the dependence on Q cancels.

For atom–diatomic mixtures, where the diatomic has an allowed vibrational transition, absorption in the null gap due to collisions primarily arises from the far wings of the lines in the monomer diatomic spectrum. Both self and foreign gas broadening contribute to the far wing absorption. The HCl self-broadening contribution was measured at room temperature as a function of pressure by Benedict *et al.*[38] These spectra were digitized and scaled for differences in HCl pressure and path length in order to remove the HCl self-broadened wings from the ArHCl spectra. Because the temperature dependence of the HCl self-broadened spectrum is not known, it cannot be reliably predicted much below room temperature.

The foreign gas broadening contribution is modeled by the line shape function used by Varanasi *et al.*[39] to an account for line wing absorption in an HCl–CO_2 mixture. The contribution of an individual monomer transition to the far wing absorption is given by

$$\sigma_{cj} = (S_j/\pi\gamma_j)(m/2)\sin(\pi/m) \times\{1 + [(\omega-\omega_j)/\gamma_j]^m\}^{-1}, \quad (19)$$

where γ_j is the foreign broadened linewidth of the jth line, S_j is the line strength, m is the line shape exponent, and ω_j is the line location. Houdeau *et al.*[40] have determined the individual widths and temperature dependences for HCl lines broadened by Ar. It is well known that in the region near the line center the shape is Lorentzian ($m = 2$), however in the far wing of a line a large deviation from Lorentz behavior is observed.[39–43] The line shape exponent has not previously been determined for Ar–HCl mixtures. We applied Eq. (18) to the Miziolek and Pimentel ArHCl spectra and found that $m = 1.85$ reasonably accounted for the observed pressure and temperature variations of the $P(1)$ and $R(0)$ line wings.

Absorption losses due to instrument optics usually vary slowly with wave number and are assumed constant over the narrow spectral extent of the ArHCl spectrum. For the multipass absorption cell used by Miziolek and Pimentel, the major loss is assumed due to imperfect mirror reflectivity, and is modeled by

$$\tau = R^n, \quad (20)$$

where R is mirror reflectivity and n is the number of passes. A value of $R = 0.991$ was found to be consistent with the observed baselines for both the Ar–HCl and He–HCl mixtures. For the single pass absorption cell used by Rank *et al.*,[16,17] the instrument loss was defined as that constant needed to bring the predicted line wing spectra into the best overall agreement with the experiment. The same value of $m = 1.85$, which was determined by the Miziolek and Pimental data, was used to predict the foreign gas broadened wings for the Rank spectra.

B. Comparison to observed spectra

The values of the spectral parameters used to calculate ArHCl spectra are summarized in Table II. An example calculation, showing representative components of the spec-

TABLE II. Summary of parameter values used in ArHCl spectral analysis.

Parameter	Value[a]
ϵ (cm^{-1})	181 (146)
B_e (cm^{-1})	0.0576 (0.075)
D_e (cm^{-1})	6.08×10^{-7} (1.10×10^{-6})
n	13 (13)
η_D	12.3 (10.3)
$\langle\cos\theta\rangle_{00}$	0.673 (0.55)
ω_b (cm^{-1})	32 (21)
α_0 (cm^{-1})	1.5×10^{-4} (1.5×10^{-4})
$\Delta\omega_0$ (cm^{-1})	−2 (−6)
V_m (cm^{-1})	76
θ_m (deg)	100
S_0 (cm^{-2} atm^{-1} at STP)	155

[a] Values for Ar–ClH configuration shown in parentheses.

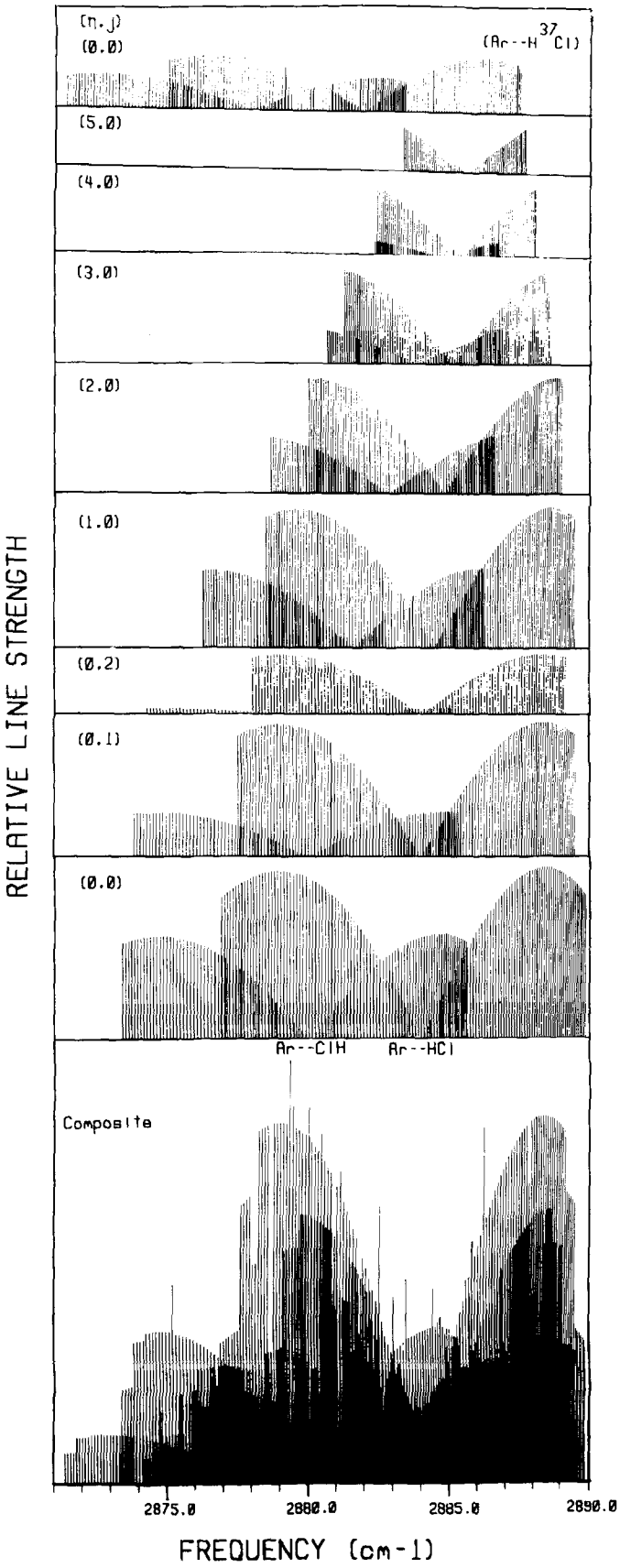

FIG. 1. Representative contributions to the ArHCl spectrum. Top spectrum for the ArH ^{37}Cl isotope. Other spectra for the ArH ^{35}Cl isotope.

trum, is presented in Fig. 1. There are separate sequences of bands for each linear configuration as well as for each isotope (ArH ^{35}Cl and ArH ^{37}Cl). Within a sequence the width of each band decreases substantially with increasing stretching and librational quantum numbers and there are sharp P and R branch cutoffs. This is due to the finite number of metastable rotational states for each stretching-librational level.

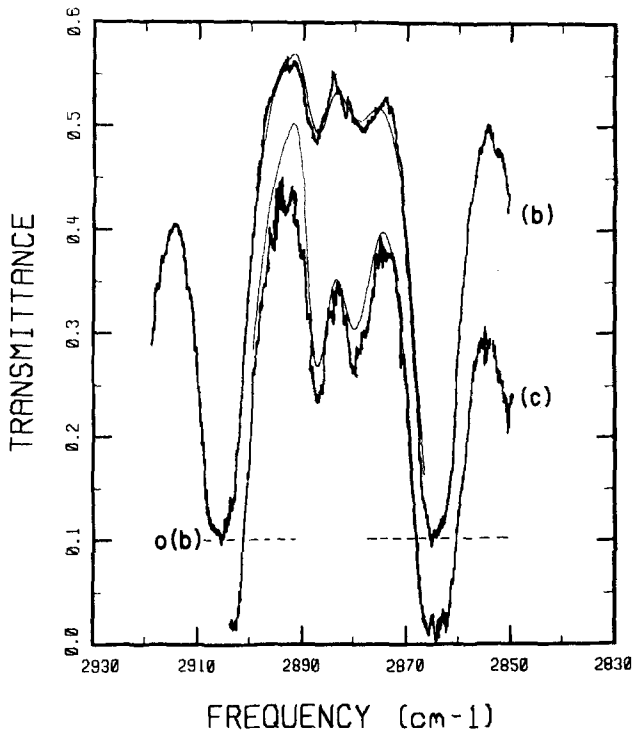

FIG. 2. Comparison of measured (—) (Miziolek and Pimentel, Ref. 18) and predicted (—) ArHCl spectra. Curve (b) displaced as indicated. (b) 298 K, 2.60 Torr HCl, 402 Torr Ar, 620 m path length. (c) 193 K, 1.28 Torr HCl, 475 Torr Ar, 460 m.

The calculated spectra were degraded with a triangular slit function to a resolution of 2.5 cm^{-1} (full width at half-maximum) in order to compare to the Miziolek and Pimentel spectra. This comparison is shown in Fig. 2. Because of the low HCl partial pressure the contribution of HCl self-broadened wings is quite small and it is reasonable to also compare to the low temperature measurement.

A 0.3 cm^{-1} slit function was used in the comparison to the spectra of Rank *et al.*[17] shown in Fig. 3. In this comparison the line wing contribution and the instrument baseline have been removed from the observed spectrum. Two predicted curves are shown, for the 181 cm^{-1} dissociation energy of the M5 potential, and for the 233 cm^{-1} value estimated by Boom and van der Elsken. It can be seen that the integrated optical depths are substantially different for the two predictions. However, uncertainties in both the absolute scale and baseline removal for the experimental curve mean it is not appropriate to choose between these two values based on this absolute intensity comparison. The point of the figure is to compare spectral shapes, which are similar to the data in both cases.

At the higher spectral resolution of this data some fine structure is evident. The source of the similar fine structure in the calculated spectrum is the sharp P and R branch cutoffs. Differences in the calculated and observed fine struc-

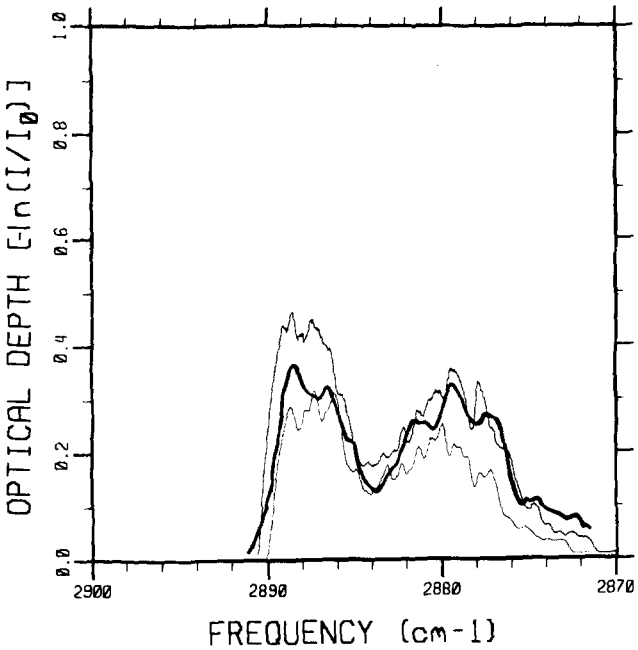

FIG. 3. Comparison of measured (—) (Rank, Rao, and Wiggins, Ref. 17) and predicted (—) ArHCl spectra: 250 Torr HCl, 5.01 atm Ar, 90 cm, 298 K. Upper curve for 233 cm^{-1} dissociation energy, lower curve for 181 cm^{-1}.

ture are likely due to model simplifications and to uncertainties in the baseline removal. It was not practical to make a quantitative comparison to the lower temperature Rank data because of the large uncertainty in removal of the HCl self-broadened component.

III. THERMODYNAMICS

Stogryn and Hirschfelder[25] used a classical method to derive useful expressions for the bound and metastable partition functions of the atom–atom complexes. Similar expressions of comparable utility are not available for atom–diatom complexes. The extra degree of freedom due to the libration of the diatomic significantly increases the complexity of a classical approach. We present a quantum mechanical approach which closely reproduces the well established atom–atom results and is straightforwardly extended to anisotropic atom–diatom potential surfaces.

A. Atom–atom systems

The quantum mechanical partition function is given by

$$Q = \sum_{\eta} \sum_{l} (2l+1)\exp(-G_{\eta l}/kT). \tag{21}$$

This function is evaluated for two summation limits corresponding to the bound and metastable limits of the orbital angular momentum l_η [see Eqs. (11) and (12)]. A useful mathematical simplification results from approximating the full expansion for the rotational energy levels contained in Eq. (3) with,

$$G_{\rm rot} = B'_\eta l(l+1). \tag{22}$$

A value of B'_η can be found which simultaneously preserves the correct total number of bound and metastable rotational levels and the correct upper limit rotational energy for each vibrational state. The proper choice is

$$B'_\eta = \xi B_e. \tag{23}$$

Substitution of $G_{\rm rot}$ in Eq. (22) and G_η in Eq. (6) into the expression for the partition function and conversion of the sum to an integral yields for the bound state limit,

$$Q_b = [(\eta_D+1)/3](\epsilon/B_e)\exp[-(1+G_0^*)/T^*]T^* \times \int_0^{1/T^*} dz(e^z-1)/z, \tag{24}$$

where $\epsilon_0 = \epsilon - G_0$, $G_0^* = G_0/\epsilon_0$, $T^* = kT/\epsilon_0$, and $z = [(\eta_D - \eta)/\eta_D]^3/T^*$. The use of this integral approximation to the partition function assumes that the mean spacing of vibrational energy levels is smaller than the thermal energy. This can be expressed by the condition $T^* > 1/\eta_D$ and for most systems applies for $T^* > 0.1$. When this condition is not met the sum resulting from substitution of Eqs. (22) and (16) into Eq. (21) should be evaluated explicitly. A simple approximation to the partition function which is accurate to within a few percent for $T^* \geqslant 0.1$ is given by

$$Q_b = [(\eta_D+1)/3](\epsilon/B_e)\exp[-(1+G_0^*)/T^*] \times \exp(0.25/T^* + 0.03/T^{*2}). \tag{25}$$

The high temperature limit of the partition function $[(\eta_D+1)/3]\times(\epsilon/B_e)$ gives the number of bound vibration-rotation states supported by the potential. The temperature dependence of the partition function derived here agrees to better than 1% with that determined by Stogryn and Hirschfelder.

Inclusion of the metastable rotational states, as in Eq. (12), results in the metastable partition function

$$Q_m = Q_b + [(\eta_D+1)/3](\epsilon/B_e)\exp[-(1+G_0^*)/T^*]T^* \times \int_0^{\delta/T^*} du(1-e^{-u})/u, \tag{26}$$

where $u = [(\eta_D - \eta)/\eta_D]^3(\delta/T^*)$.
This function can be approximated for $T^* \geqslant 0.1$ by

$$Q_m = Q_b\{1+\delta\exp[-(1+\delta)0.25/T^* - (1-\delta^2)0.03/T^{*2}]\}. \tag{27}$$

B. Atom–diatomic systems

The quantum mechanical partition function includes an additional sum over the diatomic librational states and is determined by

$$Q = \sum_{\eta}\sum_{l}\sum_{j} g_j(2l+1)\exp(-G_{nlj}/kT), \tag{28}$$

where g_j is the degeneracy of the librational level. For librational states whose energy is well above the rotational barrier, the energy and degeneracy approach the free rotor limits, $G_{\rm lib} = B_d j(j+1)$ and $g_j = 2j+1$. For librational states whose energy is comparable to or below the barrier, the energy and degeneracy do not have simple analytical forms. This is not a serious limitation for estimation of thermodynamic properties, as long as the collectively averaged energies and degeneracies can be approximated.

In order to develop a suitable approximation for the librational states we first consider the classical partition

function for a hindered rotor,

$$Q_{\rm lib} = (kT/hcB_d)\int_1^{-1} dx \exp[-V(x)/kT], \quad (29)$$

where $x = \cos\theta$. We assume a potential of the form

$$V = V_0 + V_1 x + V_2 x^2. \quad (30)$$

When this potential is constrained to match the equilibrium barrier height V_m and location x_m for the general M5 surface it can be recast as

$$V_\eta(x) = \xi^3 V_m\{1 - [(x_m - x)/(x_m - 1)]^2\}. \quad (31)$$

The quantity ξ^3 accounts for the reduction of the effective barrier height due to averaging over the stretching motion. Substitution of this potential into Eq. (29) yields the approximate result,

$$Q_{\rm lib} = (kT/hcB_d)\exp[-\beta V_\eta(x_m)/kT] \quad (32)$$

and

$$\beta = [1 - (1/3)(3x_m^2 + 1)/(x_m - 1)^2], \quad (33)$$

where it is assumed that $kT > \beta V_m$. The same librational partition function is obtained from an energy level distribution given by

$$G_{\rm lib} = E_\eta + B_d j(j+1), \quad (34)$$

where $E_\eta = \beta V_\eta(x_m)$ is the zero point rotational energy associated with each stretching state and the degeneracies are given by the free rotor values. This result can also be demonstrated by averaging the exact hindered rotor eigenvalues which originate from the same free rotor j state. Using the hindered rotor eigenvalues calculated by Boom and van der Elsken,[44] we found this approximation to apply well for both pure $\cos\theta$ and $\cos^2\theta$ potentials and for values of the rotational barrier much higher than for ArHCl. Substitution of Eq. (34) into Eq. (28) gives for the bound state partition function,

$$Q_b = [(\eta_D + 1)/3](\epsilon/B_e)(\epsilon/B_d) \times \exp[-(1 + G_0^* + E_0^*)/T^*]T^{*2} \times \int_0^{1/T^*} dz(e^z - 1 - z)/z, \quad (35)$$

where $\epsilon_0 = \epsilon - G_0 - E_0$. This function can be approximated for $T^* \geqslant 0.1$ by

$$Q_b = [(\eta_D + 1)13](\epsilon/B_e)(\epsilon/B_d) \times \exp[-(1 + G_0^* + E_0^*)/T^*]T^* \times [\exp(0.25/T^* + 0.03/T^{*2}) - 1]. \quad (36)$$

The high temperature limit of this function is the total number of bound states, and is $(1/4)[(\eta_D + 1)/3](\epsilon/B_e)(\epsilon/B_d)$.

Metastability in atom–diatomic systems can occur in two coordinates, the relative orbital angular momentum (analogous to the atom–atom system) and the diatomic librational motion. Librational metastability in ArHCl has been investigated by Ashton *et al.*[45] They calculated librational predissociative lifetimes for a large number of η, j states. For constant j, the lifetimes of the first few η states above the dissociation threshold are fairly constant at approximately 10^{-12} s, and then increase with increasing η. For fixed η, the lifetime increases with increasing j. These trends can be understood in terms of momentum gap arguments postulated by Ewing.[46,47]

Because of the variability of the librational predissociative lifetimes in atom–diatomics the calculation of the metastable partition function is not as straightforward as for atom–atom systems. An upper limit estimate can be made by not restricting the upper limit of j. Also some coupling of the orbital and librational angular motions is required because the upper limit of the orbital angular momentum depends on the disssociation energy which in turn depends on the librational state. This coupling is introduced by defining an effective dissociation energy for use in determining l_η [see Eq. (12)] given by

$$\epsilon' = \epsilon - \beta V_m. \quad (37)$$

With these approximations the metastable partition function becomes

$$Q_m = (\epsilon/B_d)T^* Q'_m, \quad (38)$$

where Q'_m is given by Eq. (27), except that the quantity G_0^* is replaced by $G_0^* + E_0^*$.

C. Thermodynamic properties

The thermodynamic properties of dimers can be calculated directly from the partition function and its derivatives. As examples we consider the heat capacity and equilibrium constant. The heat capacity can be calculated in nondimensionalized form from,[48]

$$C/R = T^{*2} d^2 \ln Q/dT^{*2} + 2T^* d \ln Q/dT^*, \quad (39)$$

where the heat capacity C is nondimensionalized in terms of the molar gas constant R. The partition functions derived earlier do not include translation which contributes an additional 3/2 to C/R. Substitution of these partition functions into Eq. (39) results in dimer heat capacity curves which are a function of reduced temperature only. The simple approximations to the partition functions presented earlier are not suitable for evaluation of the heat capacity because they do not give sufficiently accurate second derivatives. The integrals in the partition functions and their derivatives were accurately evaluated to produce the "universal" heat capacity curves shown in Figs. 4 and 5. The heat capacity curves corresponding to the bound partition function for both the atom–atom and atom–diatomic cases have a high temperature limit of zero. This is due to the finite number of bound states, which are equally populated at infinite temperature. The atom-atom metastable curve also approaches a limit of zero for the same reason. However, for metastable atom–diatomics there is no limit on the number of librational quanta which results in a high temperature limit of $C/R = 1$.

Mahan's results for the number of bound and metastable states can be combined with partition functions derived here to yield a simple and accurate representation of the equilibrium constant defined in Eq. (17). This is given by

$$K_{\rm eq} = \sqrt{2\pi} a_0(n)(4/3)\pi R_e^3 F(T^*), \quad (40)$$

where Mahan's formula for $a_0(n)$ is well approximated by

$$a_0(n) = 0.225 + 1.35/n \quad (41)$$

and the function $F(T^*)$ is given in Table III. For atom–dia-

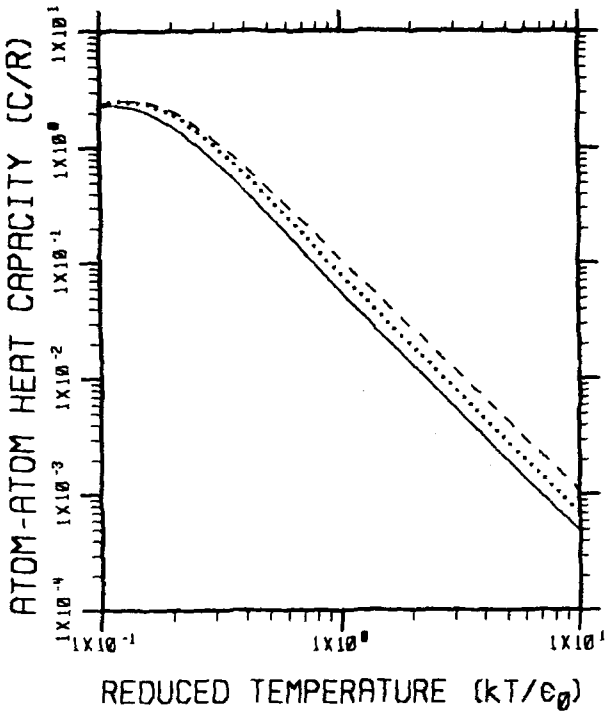

FIG. 4. Heat capacity for atom–atom systems. Bound (—). Metastable, $\delta = 0.5$ (· · ·), $\delta = 1.0$ (- -).

tom potentials with multiple minima, the value of R_e corresponding to the lowest energy minimum should be used in evaluating Eq. (40). The accuracy of this approximation for K_{eq} is established in Fig. 6 by comparison to Stogryn and Hirschfelder's predictions for Ar_2. The classical calculations are based on a reduced temperature defined by $T^* = kT/\epsilon$. This definition was adopted in comparing the quantum and classical equilibrium constants. The classical partition function does not include the reduction of the dissociation energy due to the zero point vibrational energy. This effect is incorporated in the quantum partition functions by defining the reduced temperature as $T^* = kT/\epsilon_0$. Predictions of the bound and metastable equilibrium constants for ArHCl are shown in Fig. 7.

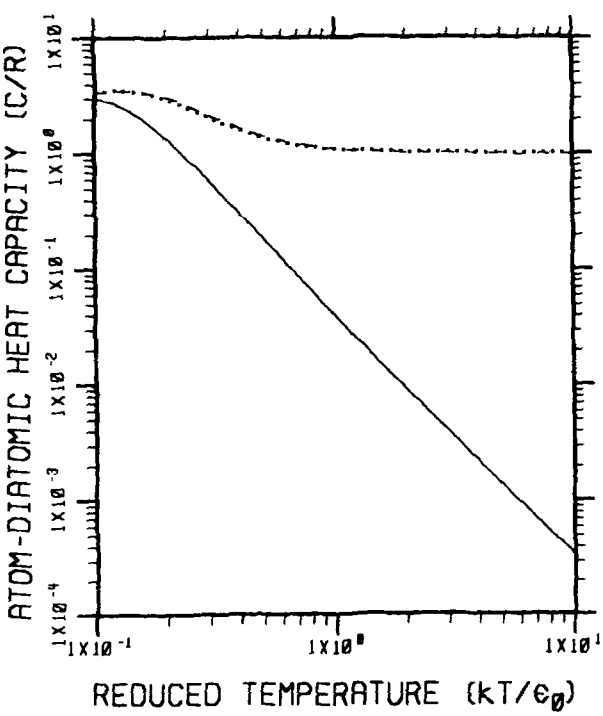

FIG. 5. Heat capacity for atom–diatomic systems. Bound(—). Metastable, $\delta = 0.5$ (· · ·) $\delta = 1.0$ (- -).

TABLE III. Definition of the function used in evaluation of the equilibrium constant.

	$X(T^*) = \exp(0.25/T^* + 0.03/T^{*2})$
Atom–Atom	
Bound:	$F = XT^{*-3/2}$
Metastable:	$F = XT^{*-3/2}\{1 + \delta \exp[-(1+\delta)0.25/T^* - (1-\delta^2)0.03/T^{*2}]\}$
Atom–Diatomic	
Bound:	$F = (X-1)T^{*-3/2}$
Metastable:	Same as for atom–atom

V. CONCLUDING REMARKS

Previous analyses[16,18,22] of ArHCl infrared spectra have been based on relating the apparent enthalpy of formation ΔH_{app} to the dissociation energy. The apparent enthalpy of formation was taken as the slope in a plot of the apparent equilibrium constant K_{app} vs reciprocal temperature where

$$K_{app} = x(\omega)/L\,[\mathrm{HCl}]\,[\mathrm{Ar}] \tag{42}$$

and

$$\ln(K_{app}) = -\Delta H_{app}/RT. \tag{43}$$

Here, $x(\omega)$ is the observed dimer optical depth (after baseline subtraction), L is pathlength in meters, [ ] is concentration in mol/l, and R is the molar gas constant. Using our spectral

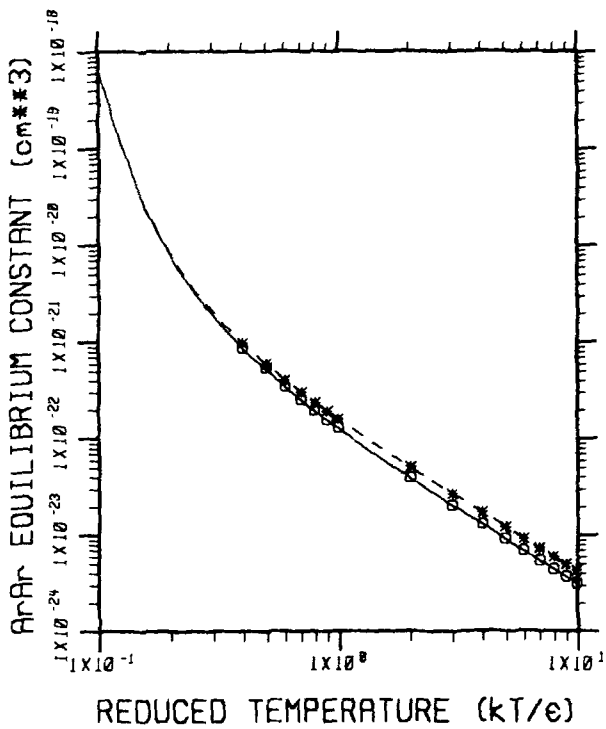

FIG. 6. Comparison of classical (Stogryn and Hirschfelder Ref. 25) and quantum equilibrium constants for Ar dimer ($\epsilon = 83.3\ \mathrm{cm}^{-1}$). Bound, present work (—), Stogryn and Hirschfelder (O). Metastable, present work (- -), Stogryn and Hirschfelder (*).

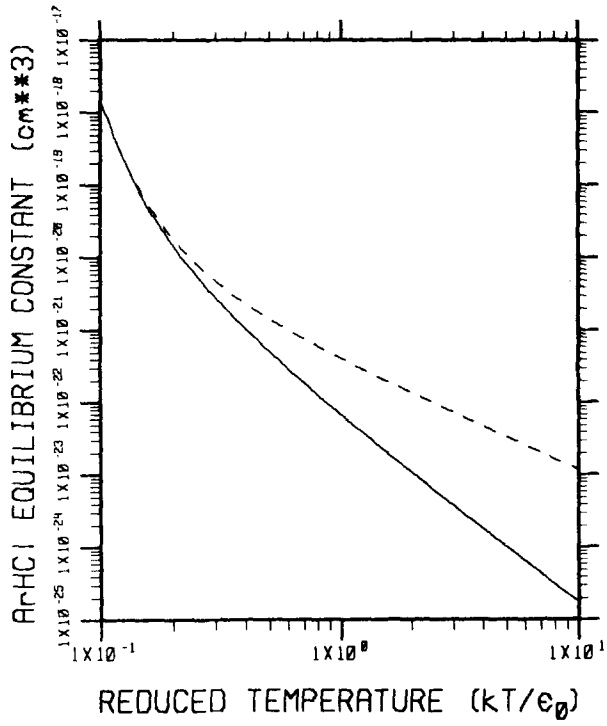

FIG. 7. Predicted equilibrium constants for ArHCl ($\epsilon_0 = 117$ cm^{-1}). Bound (—). Metastable (- -).

model, we can compare directly to the Miziolek–Pimentel data,[18] which is shown in Fig. 8. On the basis of simply comparing calculated and observed values for ΔH_{app} it is not possible to strongly prefer one dissociation energy over the other. However, the absolute values of K_{app} for the higher dissociation energy,[22] $\epsilon = 233$ cm^{-1}, are substantially above the data and correspond to about 50% more dimer optical depth than was observed.

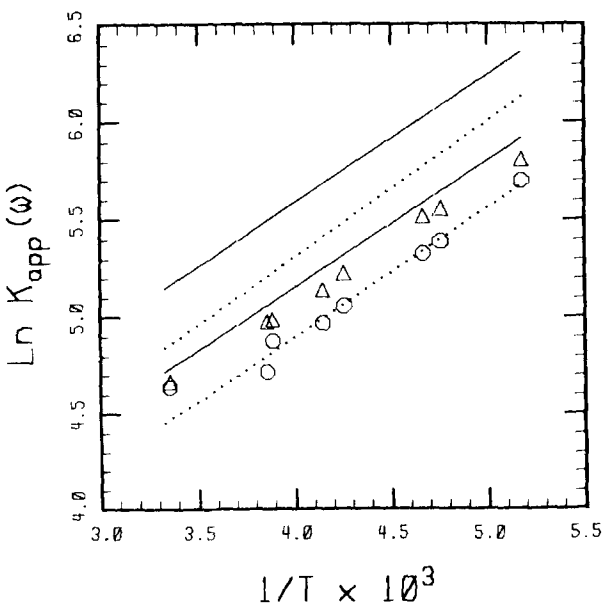

FIG. 8. Comparison of predicted and observed apparent equilibrium constant. Miziolek–Pimentel data (Ref. 18) at 2879 cm^{-1} (O) and 2887 cm^{-1} (△). Data error bars are approximately equal to the symbol height. Predicted at 2879 cm^{-1} (· · ·) and 2887 cm^{-1} (—). Upper pair of predicted curves for $\epsilon = 233$ cm^{-1} and lower pair for $\epsilon = 181$ cm^{-1}.

The spectral model developed here can be applied to any atom–linear molecule system with potential minima corresponding to linear structures. This approach can be generalized for nonlinear configurations by modeling the spectra as the sum of parallel and perpendicular bands of a prolate symmetric top. Similarly, the partition functions and derived thermodynamic properties apply with complete generality to atom–linear molecule systems. This also holds true for van der Waals molecules with a nonlinear equilibrium geometry as long as the hindering potential can be approximated by Eq. (30).

Note added in proof: The thermodynamic behavior of any molecule is a strong function of the reduced temperature $T^* = kT/\epsilon_0$. It is expected that diatomic molecules at high temperature and van der Waals dimers at room temperature will have a comparable T^* and therefore exhibit similar thermodynamic behavior. This similarity has been noted recently by F. H. Mies and P. S. Julienne [J. Chem. Phys. **77**, 6162 (1982)] and J. Tellinghuisen [Chem. Phys. Lett. **102**, 4 (1983)]. Additionally, Tellinghuisen evaluated the exact quantum mechanical partition function for Ar_2, where the ratio of metastable to bound states corresponds to that predicted by Mahan.[26]

ACKNOWLEDGMENTS

The authors thank the Atmospheric Sciences Division of the National Science Foundation for sponsoring this work. Discussions with Professor J. Calo, Professor R. Andres, and Dr. C. E. Kolb are gratefully acknowledged. The authors also thank the reviewer for suggesting improvements to this work.

[1] R. J. LeRoy and J. Van Kranendonk, J. Chem.Phys. **61**, 4750 (1974).
[2] H. Kreek and R. J. LeRoy, J. Chem. Phys. **63**, 338 (1975).
[3] J. K. Cashion, J. Chem. Phys. **45**, 1656 (1966).
[4] G. Henderson and G. E. Ewing, Mol. Phys. **27**, 903 (1974).
[5] R. G. Gordon and J. K. Cashion, J. Chem. Phys. **44**, 1190 (1966).
[6] G. Henderson and G. E. Ewing, J. Chem. Phys. **59**, 2280 (1973).
[7] A. Watanabe and H. L. Welsh, Phys. Rev. Lett. **13**, 810 (1964).
[8] A. Kudian, H. L. Welsh, and A. Watanabe, J. Chem. Phys. **43**, 3397 (1965).
[9] A. Kudian, H. L. Welsh, and A. Watanabe, J. Chem. Phys. **47**, 1553 (1967)
[10] A. Kudian, and H. L. Welsh, Can. J. Phys.**49**, 230 (1971).
[11] A. R. W. McKellar and H. L. Welsh, J. Chem. Phys. **55**, 595 (1971).
[12] A. R. W. McKellar and H. L. Welsh, Can. J. Phys. **50**, 1458 (1972)
[13] A. R. W. McKellar and H. L. Welsh, Can. J. Phys. 52, 1082 (1974).
[14] R. D. Pendley and G. Ewing J. Chem. Phys. **78**, 3531 (1983).
[15] C. A. Long and G. E. Ewing, J. Chem. Phys. **58**, 4824 (1973).
[16] D. H. Rank, P. Sitaram, W. A. Glickman, and T. A. Wiggins, J. Chem. Phys. **39**, 2673 (1963).
[17] D. H. Rank, B. S. Rao, and T. A. Wiggins, J. Chem. Phys. **37**, 2511 (1962).
[18] A. W. Miziolek and G. C. Pimentel, J. Chem. Phys. **65**, 4462 (1976).
[19] M. Larvor, J.P. Houdeau, and C. Haeusler, Spectrochim. Acta Part A **29**, 971 (1973).
[20] J. M. Hutson and B. J. Howard, Mol. Phys. **45**, 769 (1982).
[21] J. M. Hutson and B. J. Howard, Mol. Phys. **43**, 493 (1981).
[22] E. W. Boom and J. Van der Elsken, J. Chem. Phys. **77**, 625 (1982).
[23] E. W. Boom, D. Frenkel, and J. van der Elsken, J. Chem. Phys. **66**, 1826 (1977).
[24] E. W. Boom, and J. van der Elsken, J. Chem. Phys. **73**, 15 (1980).
[25] D. E. Stogryn and J. O. Hirschfelder, J. Chem. Phys. **31**, 1531 (1959).
[26] G. D. Mahan, J. Chem. Phys. **52**, 258 (1970).
[27] J. K. Cashion, J. Chem. Phys. **48**, 94 (1968).
[28] R. J. LeRoy, Chem. Phys. Lett. **67**, 207 (1979).
[29] S. L. Holmgren, M. Waldman, and W. Klemperer, J. Chem. Phys. **67**, 4414 (1977).

[30]S. L. Holmgren, M. Waldman, and W. Klemperer, J. Chem. Phys. **69**, 1661 (1978).
[31]A. M. Dunker and R. G. Gordon, J. Chem. Phys. **64**, 354 (1976).
[32]I. F. Kidd, G. G. Balint-Kurti, and M. Shapiro, Faraday Discuss. Chem. Soc. **73**, 287 (1983).
[33]R. J. LeRoy and J. Scott Carley, Adv. Chem. Phys. **42**, 353 (1980).
[34]S. Bratoz and M. L. Martin, J. Chem. Phys. **42**, 1051 (1965).
[35]G. Herzberg, *Spectra of Diatomic Molecules* (van Nostrand, New York 1966).
[36]R. J. LeRoy and R. B. Bernstein, J. Chem. Phys. **52**, 3869 (1970).
[37]*Vibrational Spectroscopy of Trapped Species*, edited by H. E. Hallam (Wiley, New York, 1973).
[38]W. S. Benedict, R. Herman, G. E. Moore, and S. Silverman, Can. J. Phys. **34**, 850 (1956).
[39]P. Varanasi, S. K. Sarangi, and G. D. T. Tejwani, J. Quant.Spectrosc. Radiat. Transfer **12**, 857 (1972).
[40]J. P. Houdeau, M. Larvor, and C. Haeusler, J. Quant. Spectrosc. Radiat. Transfer **16**, 457 (1976).
[41]S. A. Clough, F. X. Kneizys, R. Davies, R. Gamache, R. Tipping, A. Deepak, T. D. Wilkerson, and L. H. Ruhnke, in *Atmospheric Water Vapor* (Academic, New York, 1980).
[42]R. Kubo in, *Lectures in Theoretical Physics*, edited by W. E. Brittin and L. G. Dunham (Interscience, New York 1959), Vol. I, p. 186.
[43]A. Ben-Reuven, Adv. Chem. Phys. **33**, 235 (1975).
[44]E. W. Boom, Ph.D. thesis, University of Amsterdam, June 1981.
[45]C. J. Ashton, M. S. Child, and J. M. Hutson, J. Chem. Phys. **78**, 4025 (1983).
[46]G. E. Ewing, J. Chem. Phys. **73**, 325 (1980).
[47]G. E. Ewing, J. Chem. Phys. **72**, 2096 (1980).
[48]G. N. Lewis, M. Randall, K. S. Pitzer, and L. Brewer, *Thermodynamics*, 2nd ed. (McGraw–Hill New York, 1961).